Aeroacoustics Conferences
June 4-7, 2024, Rome, Italy
30th AIAA/CEAS Aeroacoustics Conference (2024)

10.2514/6.2024-3031

Properties of the tones emerging in the near-nozzle pressure spectra of hot high-speed jets

Christophe Bogey*
CNRS, Ecole Centrale de Lyon, INSA Lyon, Universite Claude Bernard Lyon I,
Laboratoire de Mécanique des Fluides et d'Acoustique, UMR 5509, 69130 Ecully, France

The influence of temperature on the acoustic tones emerging in the near-nozzle pressure spectra of high-speed jets is investigated using large-eddy simulations. The jets have nozzle-exit temperatures equal to 1, 1.5 and 2.25 times the ambient temperature and velocities yielding acoustic and jet Mach numbers M_a and M_j, relative to the speeds of sound in the ambient medium and in the jet flow, respectively, between $M_a = 0.30$ and 2 and between $M_j \simeq 0.50$ and 1.5. For the hot jets, acoustic tones appear near the nozzle for sufficiently high nozzle-exit velocities, as for the isothermal jets. As the jet temperature increases, at a fixed acoustic Mach number, the tones are weaker and appear at higher Strouhal numbers. At a fixed jet Mach number, on the contrary, their characteristics do not change much. However, their levels increase by a few dB, their Strouhal numbers slightly decrease, and for $M_j < 1$ their widths are larger. These results are consistent with the properties of the upstream-propagating free-stream guided jet waves for a vortex-sheet model. Finally, at a fixed jet Mach number, the tone prominence does not vary significantly with the temperature, suggesting that the mechanisms responsible for the tones are of same nature and of similar strength in isothermal and hot jets.

I. Introduction

The presence of acoustic tones of physical nature in the near pressure field of high-speed jets has been recognized for less than ten years since the studies of Towne et al. [1] and Brès et al. [2]. These authors demonstrated that these tones, first documented in Suzuki and Colonius [3] in 2006, are related to the existence of guided jet waves (GJW), whose properties were described theoretically in the late eighties by Tam and Hu [4]. The GJW are essentially confined inside the jet potential core and can travel in the upstream or in the downstream directions. The GJW which travel upstream and have significant amplitude in the jet shear layer and outside the flow, hereafter called upstream-propagating free-stream GJW, are of particular interest. These waves, allowed only inside limited frequency bands, have been shown in Tam and Ahuja [5], Bogey and Gojon [6], Jordan et al. [7], Gojon et al. [8], Edgington-Mitchell [9] and Mancinelli et al. [10], among others, to be involved in the feedback mechanisms establishing in impinging and screeching jets, producing intense acoustic tones. For high-speed non-screeching free jets, they also lead to the generation of tones near the jet nozzle exit as reported in Towne et al. [1], Brès et al. [2], Bogey [11] and Zaman et al. [12], and in the jet acoustic far field in the upstream direction as highlighted in Bogey [13] and Zaman et al. [14]. In subsonic and nearly perfectly expanded supersonic free jets with laminar nozzle-exit conditions, they were also found in Bogey [15] to excite the shear-layer instability waves near the nozzle.

Most studies on near-nozzle acoustic tones in free jets have been performed for cold or isothermal jets and very few dealt with hot jets. However, the theoretical works by Towne et al. [1] and by Edgington-Mitchell and Nogueira [16] and the experimental results of Upadhyay and Zaman [17] can be mentioned. First, based on the properties of the GJW predicted using a vortex-sheet model, Towne et al. [1] suggested that for high-subsonic hot jets, near-nozzle acoustic tones should persist above a jet Mach number increasing with jet temperature. Their predictions were noted to be consistent with the experimental data obtained by Suzuki and Colonius [3] in the near pressure fields of hot jets. More recently, Edgington-Mitchell and Nogueira [16] investigated the sensitivity of the frequency bands of the upstream-propagating GJW to different jet parameters, including temperature, using a finite-thickness linear stability code. At a fixed jet Mach number between 0.90 and 1.80, for a higher temperature, the bands were found to move to lower Strouhal numbers and to be slightly wider, in most cases. Finally, in the experiments of Upadhyay and Zaman [17], acoustic tones were measured near the nozzle of jets at Mach numbers between 0.60 and 1.40 at least up to a jet stagnation temperature of 473 K. At a given jet Mach number, the tone Strouhal numbers were observed to decrease with increasing jet temperature with no notable change occurring in their amplitudes.

*CNRS Research Scientist, christophe.bogey@ec-lyon.fr, AIAA Senior Member & Associate Fellow.

Considering the above, there is clearly a need for a more detailed description of the influence of jet temperature on the acoustic tones emerging in the near-nozzle pressure spectra of high-speed non-screeching jets. This is done in the present paper from data obtained for isothermal and hot round free jets using well-resolved large-eddy simulations (LES). The hot jets have temperatures equal to 1.5 and 2.25 times the ambient temperature. At the nozzle exit, the jets have fully laminar or highly disturbed nozzle-exit boundary layers and velocities yielding acoustic Mach numbers relative to the ambient speed of sound ranging from 0.30 up to 2. The presence of tonal components will be sought in the pressure spectra calculated near the nozzle lip just outside the jet flow. The main tone characteristics, namely their Strouhal numbers, amplitudes, widths and prominences, will be described. Their variations with the jet temperature, depending on the jet velocity and Mach number, will be discussed. They will also be compared with those expected on the basis of the properties of the upstream-propagating free-stream GJW for a vortex-sheet model. The present results should allow us to determine whether the near-nozzle acoustic tones obtained in isothermal and hot jets differ or not, in terms of nature and strength notably. This is an important issue given the key role played by the waves producing these tones in the feedback mechanisms arising in jets.

The paper is organized as follows. In section II, the jet initial conditions and the LES methods and parameters are documented. In section III, vorticity and pressure snapshots are first displayed. Afterwards, the main characteristics of the acoustic tones in the near-nozzle pressure spectra are presented. The effects of the temperature on the tones are discussed at a fixed acoustic Mach number, then at a fixed jet Mach number. Finally, concluding remarks are given in section IV.

II. Parameters

A. Jet flow conditions

The jets considered in this work are represented in figures 1(a-b) as a function of their nozzle-exit velocities u_j and static temperatures T_j. Their acoustic Mach numbers $M_a = u_j/c_a$ vary between 0.30 and 2, their Reynolds numbers $\mathrm{Re}_D = u_j D/\nu_j$ are all set to 100, 000 and their temperatures are equal to T_a, $1.5T_a$ and $2.25T_a$, where $D = 2r_0$, c_a, c_j, ν_j and T_a are the nozzle diameter, the speeds of sound in the ambient medium and in the jet flow, the kinematic molecular viscosity in the jet and the ambient temperature. They originate at $z = 0$ from a pipe nozzle of radius $r_0 = D/2$ and length $2r_0$, whose lip is $0.05r_0$ thick, into a medium at rest at $T_a = 293$ K and $p_a = 10^5$ Pa. At the pipe inlet, Blasius laminar boundary-layer profiles of thickness δ_{BL} are imposed for the axial velocity [18], radial and azimuthal velocities are set to zero, pressure is equal to p_a and temperature is determined by a Crocco-Busemann relation.

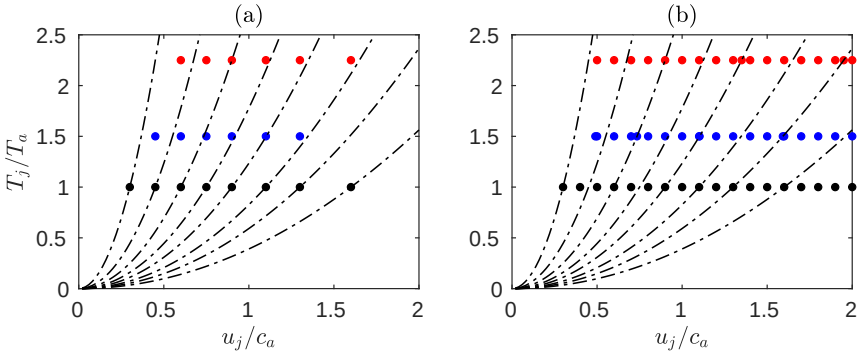

Fig. 1 Nozzle-exit velocities u_j and temperatures T_j of the jets with (a) tripped and (b) untripped boundary layers at • $T_j = T_a$, • $T_j = 1.5T_a$ and • $T_j = 2.25T_a$; − · − · isocontours for $M_j = 0.30$, 0.45, 0.60, 0.75, 0.90, 1.10, 1.30 and 1.60, from left to right.

In the pipe nozzle, the boundary layers are tripped for the jets in figure 1(a) but untripped for those in figure 1(b), in order to obtain highly disturbed and fully laminar flow conditions at the exit, respectively. For the tripped jets, the boundary layers, of thickness $\delta_{BL} = 0.15r_0$ at the pipe inlet, are forced at $z \simeq -r_0$ by adding random vortical disturbances of magnitude adjusted to reach the desired level of turbulent intensity at the exit [18, 19]. For all jets, the procedure yields a mean velocity profile similar to a Blasius laminar boundary-layer profile of momentum thickness

$\delta_\theta = 0.018r_0$ and a peak root-mean-square value u'_e of axial velocity fluctuations close to $0.09u_j$ at the nozzle exit. For the untripped jets, the boundary-layer profiles in the pipe have a thickness $\delta_{BL} = 0.10r_0$, corresponding to $\delta_\theta = 0.012r_0$, and the nozzle-exit rms velocity fluctuations u'_e do not exceed $0.002u_j$. It can noted that results obtained for the isothermal jets can be found in previous papers, namely in Bogey [11] for the tripped jets and in [15] for the untripped jets.

The acoustic Mach numbers of the twenty tripped jets in figure 1(a) are equal to $M_a = 0.3$, 0.45, 0.60, 0.75, 0.90, 1.1, 1.3 and 1.6. Those of the more than fifty untripped jets in figure 1(b) range typically between 0.5 and 2 in increment of 0.1. Due to the fact that the speed of sound c_j in the jet with $T_j > T_a$ is higher than c_a, the Mach numbers $M_j = u_j/c_j$ of the hot jets are lower than their acoustic Mach numbers, as illustrated by the isocontours of M_j in figure 1. Thus, for example, the two hot jets at $M_a = 0.90$ with $T_j = 1.5T_a$ and $2.25T_a$ in figure 1(a) have Mach numbers $M_j = 0.73$ and 0.60, respectively. On the contrary, the three jets at $M_a = 0.90$ with $T_j = T_a$, at $M_a = 1.10$ with $T_j = 1.5T_a$ and at $M_a = 1.30$ with $T_j = 2.25T_a$ all have a Mach number $M_j \simeq 0.90$. Thus, in what follows, the results can compared at a fixed acoustic Mach number (or jet velocity) and at a fixed jet Mach number.

B. Numerical methods

The jets are computed using the same framework as in previous jet simulations of the author [11, 15, 18, 20]. The LES are carried out by solving the three-dimensional compressible Navier-Stokes equations in cylindrical coordinates (r, θ, z) using low-dissipation and low-dispersion explicit schemes. The axis singularity is taken into account by the method of Mohseni and Colonius [21]. In order to alleviate the time-step restriction near the cylindrical origin, the derivatives in the azimuthal direction around the axis are calculated at coarser resolutions than permitted by the grid [22]. For the points closest to the jet axis, they are evaluated using 16 points, yielding an effective resolution of $2\pi/16$. Fourth-order eleven-point centered finite differences are used for spatial discretization, and a second-order six-stage Runge-Kutta algorithm is implemented for time integration [23]. A sixth-order eleven-point centered filter [24] is applied explicitly to the flow variables every time step. Non-centered finite differences and filters are also used near the pipe walls and the grid boundaries [25, 26]. The explicit filtering is employed to remove grid-to-grid oscillations, but also, as the mesh grid is not fine enough to compute the smallest turbulent structures, as a subgrid-scale high-order dissipation model in order to relax turbulent energy from scales at wave numbers close to the grid cut-off wave number while leaving larger scales mostly unaffected. The performance of this LES approach has been assessed in past studies for subsonic jets, Taylor-Green vortices and turbulent channel flows [27–29]. At the boundaries, the radiation conditions of Tam and Dong [30] are applied, with the addition at the outflow of a sponge zone combining grid stretching and Laplacian filtering in order to avoid significant acoustic reflections. Small adjustment terms are also added to prevent that mean density and pressure deviate significantly from ambient density and pressure, and no co-flow is imposed. Finally, for the jets with untripped boundary layers at $M_j \geq 1.30$, a shock-capturing filtering is applied in order to avoid Gibbs oscillations near the weak shock cells forming in their potential cores. It consists in applying a conservative second-order filter at a magnitude determined each time step using a shock sensor [24].

C. Simulation parameters

The LES grids are detailed in a previous paper [11]. They derive from the one constructed in a grid-sensitivity study [20]. In the azimuthal direction, there are $N_\theta = 1,024$ points for the tripped jets and $N_\theta = 256$ for the untripped jets. In the (r, z) section, the same reference grid is used for all jets, except for the tripped jets at $M_a > 1.30$. It contains $N_r = 512$ points in the radial direction and $N_z = 2,085$ points in the axial direction. Its physical extents are $L_r = 15r_0$ and $L_z = 40r_0$. The minimum mesh spacings are equal to $\Delta r = 0.0036r_0$ around $r = r_0$ and to $\Delta z = 0.0072r_0$ at $z = 0$. The maximal mesh spacings are equal to $\Delta r = 0.075r_0$ for $r \geq 6.25r_0$, and $\Delta z = 0.049r_0$ at $z = L_z$. For the tripped jets at $M_a > 1.30$, a finer and larger grid, containing $N_r = 572$ and $N_z = 2,412$ points, is used. In the radial direction, the mesh spacing Δr is identical to the reference grid for $r \leq 4r_0$, but is equal to $0.05r_0$ for $r \geq 4r_0$. In the axial direction, the grid also coincides with the reference grid for $z \leq 0$. Downstream of the nozzle exit, it is stretched to obtain $\Delta z = 0.053r_0$ at $z = L_z = 50r_0$.

The simulations have been performed with an OpenMP-based in-house solver. In order to ensure numerical stability, the time step used is given by $\Delta t = CFL \times \min(\Delta r)/c_a$ with $CFL = 0.70$ for all jets, except for the tripped jets at $M_a \leq 0.75$. In the latter cases, the values of the CFL numbers are larger to reduce computational cost, and increase up to $CFL = 1.30$ for the isothermal jet at a Mach number of 0.30. The time T of the simulations after the flow transient period varies from $500r_0/u_j$ for the untripped jets up to approximately $4,000r_0/u_j$ for most of the tripped isothermal jets. It is of the order of $1,500r_0/u_j$ for the tripped hot jets. During time T, density, velocity components

and pressure have been recorded at several locations, refer to reference [31] for an exhaustive description of the data available. The data of interest in this work include those in the nozzle-exit plane at $z = 0$, which have been stored at a sampling frequency corresponding to a Strouhal number $St_D = fD/u_j = 12.8$, where f is the frequency, with 256 points in the azimuthal direction. The signals have also been acquired in the azimuthal planes at $\theta = 0$, $\pi/4$, $\pi/2$ and $3\pi/4$ at a sampling frequency of $St_D = 6.4$. The Fourier coefficients estimated over the section (r, z) have been saved in the same way for the azimuthal modes $n_\theta = 0$ to 8 for the tripped jets and from $n_\theta = 0$ to 2 for the untripped jets. The statistics are averaged in the azimuthal direction, when possible. The time spectra are evaluated from overlapping samples of duration $90r_0/u_j$.

III. Results

A. Vorticity and pressure snapshots

Snapshots of the vorticity norm and of the pressure fluctuations obtained in the (z, r) plane in the vicinity of the nozzle for the tripped jets at $T_j = T_a$ and $T_j = 2.25T_a$ are provided in figures 2(a-c) and 2(d-f) for the acoustic Mach numbers $M_a = 0.75$, $M_a = 0.90$ and $M_a = 1.10$, from left to right. Vorticity and pressure fields calculated for the tripped jets at $T_j = T_a$ and $T_j = 2.25T_a$ with $M_j \simeq 0.75$, $M_j \simeq 0.90$ and $M_j \simeq 1.10$ are represented in figures 3(a-c) and 3(d-f) in the same manner.

In the vorticity fields, in all cases, the jet mixing layers exhibit turbulent structures near the nozzle lip due to the highly-disturbed nozzle-exit flow conditions. Farther downstream, they develop and contain large-scale structures as well as fine-scale turbulence. In both figures, the shear-layer development is slower as the jet velocity increases, and is faster for $T_j = 2.25T_a$ than for $T_j = T_a$. These results are consistent with the influence of jet velocity and temperature on the growth rates of Kelvin-Helmholtz instability waves predicted by linear stability analysis [32, 33].

In the pressure fields, low-frequency hydrodynamic disturbances associated with the flow large-scale structures are visible on both sides of the shear layers [34]. Weak shock cells can also be detected in the core of the supersonic jets, see for instance in figure 2(c), despite that ambient pressure is imposed at the inlet of the pipe nozzle. More importantly, acoustic waves can be seen outside the jet flow but also inside the potential core. The waves in the jets are most likely GJW. For a given acoustic Mach number, in figure 2, they clearly appear to have lower amplitudes and longer wavelengths in the hot jet than in the isothermal one. For a given acoustic Mach number, in figure 3, different trends are observed. In that case, the amplitudes of the GJW may be slightly stronger for $T_j = 2.25T_a$ than for $T_j = T_a$, and their wavelengths look similar for the two temperatures.

In what follows, based on these results, the effects of jet temperature on the properties of the acoustic tones possibly emerging in near-nozzle region of the jets are examined by comparing the pressure spectra obtained at $z = 0$ and $r = 1.5r_0$ first for a fixed acoustic Mach number M_a (and jet velocity u_j), then for a fixed jet Mach number M_j.

B. Near-nozzle tone properties at a fixed acoustic Mach number

The near-nozzle spectra obtained for the tripped jets at acoustic Mach numbers $M_a = 0.75$, $M_a = 0.90$ and $M_a = 1.10$ are represented in figures 4(a-c) as a function of St_D. As for the isothermal jets [11], peaks can be seen in the spectra for the hot jets for a sufficiently high jet velocity. However, the jet velocity above which they appear increases with the temperature, yielding threshold acoustic Mach numbers varying approximately from $M_a = 0.75$ for $T_j = T_a$ up to $M_a = 1.10$ for $T_j = 2.25T_a$. Consequently, for a given jet velocity, the acoustic peaks are less intense and broader for a higher temperature, as illustrated in figure 4(c) for $M_a = 1.10$ for instance. They are also found at higher Strouhal numbers.

To understand the reason for the changes in the peak properties with the jet temperature mentioned above, the Strouhal numbers of the first three peaks obtained for the tripped jets at $T_j = T_a$, $T_j = 1.5T_a$ and $T_j = 2.25T_a$ for the azimuthal mode $n_\theta = 1$, for instance, are represented in figures 5(a-c) as a function of M_a between $M_a = 0.60$ and $M_a = 1.30$. In all cases, they are located inside or very close to the allowable frequency bands of the first radial modes of the free-stream upstream-propagating GJW predicted using a vortex-sheet model, highlighted in grey, with a dominant peak in the band of the radial mode $n_r = 1$, in agreement with previous studies [1, 2, 11, 15]. As the jet temperature rises, these bands are thicker and move to higher Strouhal numbers, leading to the right shift of the peaks in the spectra of figure 4 . In figure 5, the upper limits of the GJW bands are displayed in red or in green, as they correspond, respectively, to stationary GJW with zero group velocity or to the least-dispersed GJW when stationary GJW do not exist [11]. For all bands, the changeover from a least-dispersed GJW limit to a stationary GJW limit occurs

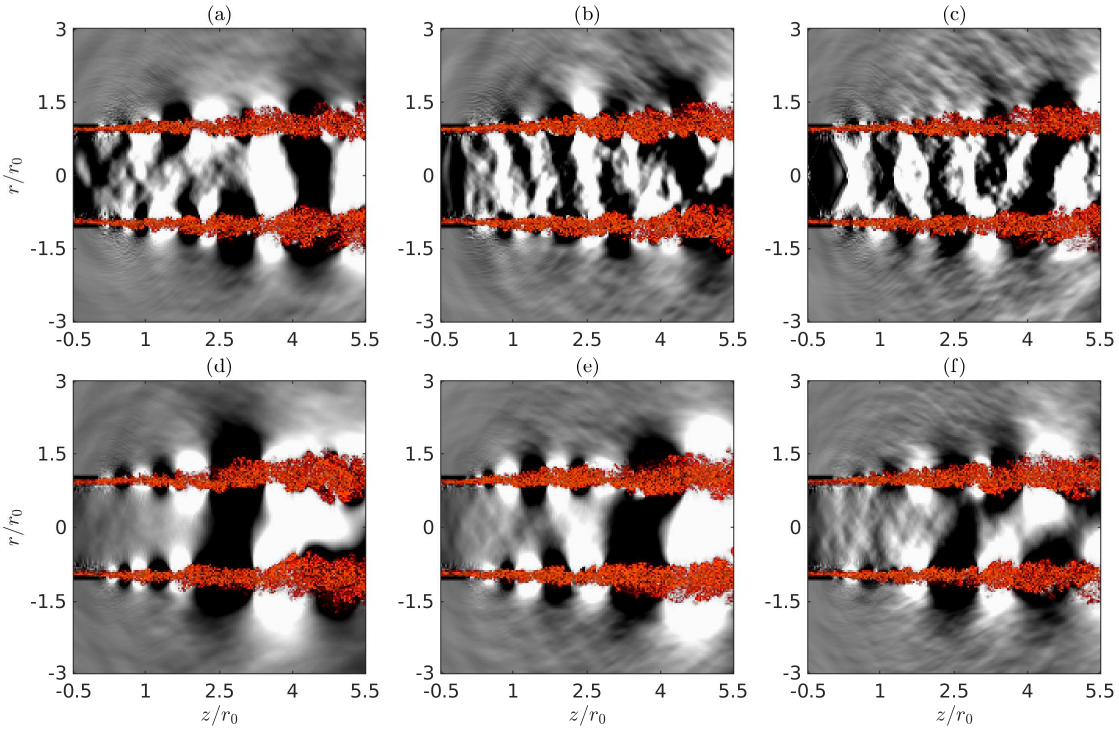

Fig. 2 Vorticity norm and pressure fluctuations for the tripped jets (a-c) $T_j = T_a$ and (d-f) $T_j = 2.25T_a$ with (a,d) $M_a = 0.75$, (b,e) $M_a = 0.90$ and (c,f) $M_a = 1.10$. For vorticity, the color scale levels range from 0 to $12u_j/r_0$, from white to red; for pressure, the grey scale levels range between (left) $\pm 2 \times 10^{-3} p_a$, (middle) $\pm 3 \times 10^{-3} p_a$ and (right) $\pm 5 \times 10^{-3} p_a$.

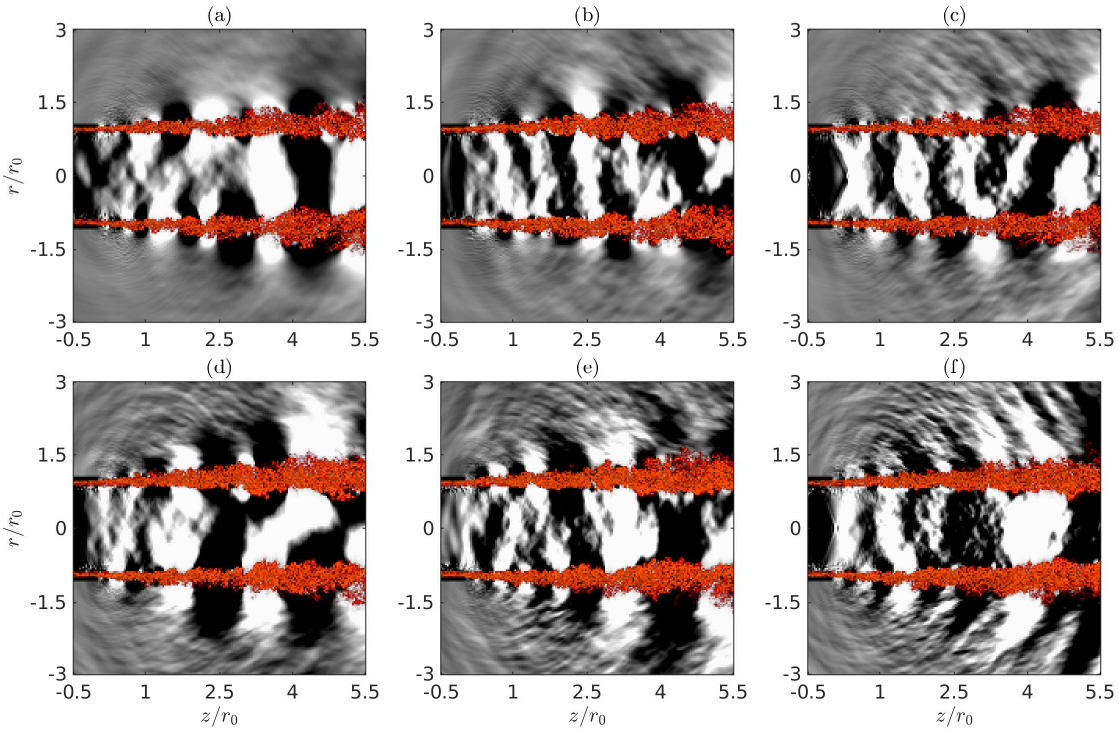

Fig. 3 Vorticity norm and pressure fluctuations for the tripped jets at (a-c) $T_j = T_a$ and (d-f) $T_j = 2.25T_a$ with (a,d) $M_j \simeq 0.75$, (b,e) $M_j \simeq 0.90$ and (c,f) $M_j \simeq 1.10$. Same color scales as in figure 2.

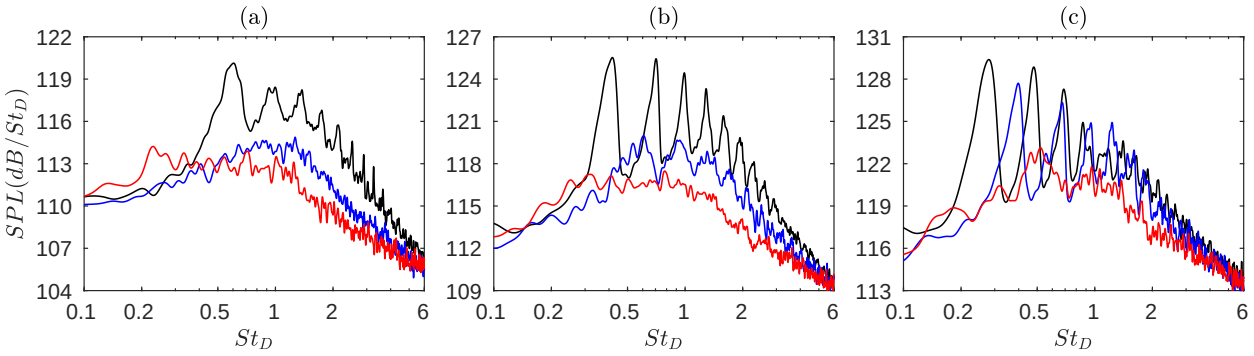

Fig. 4 Sound pressure levels at $z = 0$ and $r = 1.5r_0$ for the tripped jets at (a) $M_a = 0.75$, (b) $M_a = 0.90$ and (c) $M_a = 1.10$ as a function of St_D: ——— $T_j = T_a$, ——— $T_j = 1.5T_a$ and ——— $T_j = 2.25T_a$.

at a much higher acoustic Mach number with increasing jet temperature. Given that the near-nozzle peaks are expected to be weak and broadband, if not absent, in the first case, but to be strong and tonal in the second case [1, 11], this explains the lesser intensity and prominence of the peaks for the hot jets in figure 4. Thus, the significant variations of the Strouhal numbers and degrees of emergence of the near-nozzle peaks with the jet temperature observed for a fixed acoustic Mach number result from those of the characteristics of the GJW modes.

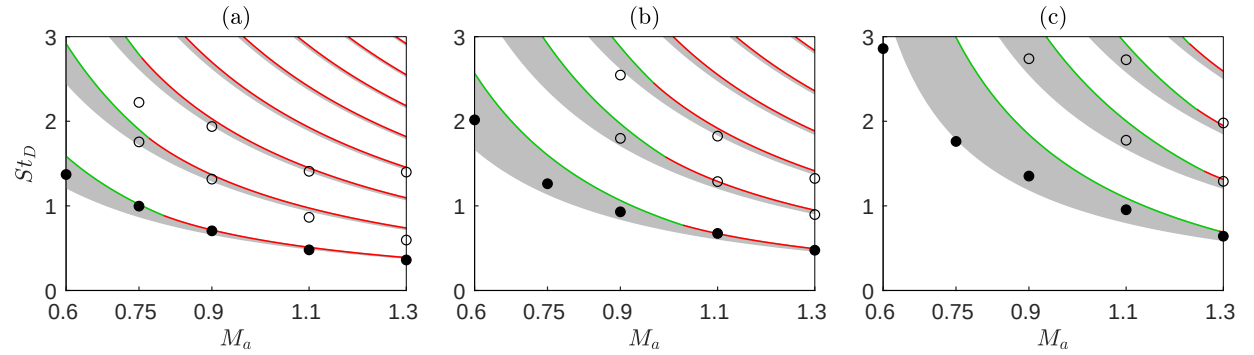

Fig. 5 Variations with M_a of the peak Strouhal numbers in the pressure spectra at $z = 0$ and $r = 1.5r_0$ for the tripped jets with (a) $T_j = T_a$, (b) $T_j = 1.5T_a$ and (c) $T_j = 2.25T_a$ for $n_\theta = 1$: • dominant and ∘ second and third strongest peaks; (grey) frequency bands of the free-stream upstream-propagating GJW, upper limits of the bands corresponding to ——— stationary and ——— least-dispersed GJW.

C. Near-nozzle tone properties at a fixed jet Mach number

The properties of the near-nozzle peaks are now examined for a fixed jet flow Mach number M_j. First, the pressure spectra obtained at $z = 0$ and $r = 1.5r_0$ for the tripped jets at $M_j \simeq 0.75$, $M_j \simeq 0.90$ and $M_j \simeq 1.10$ and for the untripped jets at $M_j = 0.60$, $M_j = 0.90$ and $M_j = 1.30$ are plotted in figures 6(a-c) and 7(a-c), respectively, as a function of St_D. In all cases, they show similar features for the isothermal jets and the hot jets. For the jets at $M_j \geq 0.90$, in figures 6(b,c) and 7(b,c), they exhibit tones of same shape at comparable Strouhal numbers regardless the jet temperature. With increasing temperature, however, the Strouhal numbers of the tones slightly decrease and their levels strenghten by a few dB. For the tripped jets at $M_j \simeq 0.75$, in figure 6(a), the spectra all contain broadband peaks, whose Strouhal numbers and levels vary with the jet temperature similarly to those of the tones at higher Mach numbers. Finally, for the untripped jets at $M_j = 0.60$, in figure 7(a), no peaks clearly appear in the spectra for $T_j = T_a$ and $T_j = 2.25T_a$ and one tone emerges around $St_D = 1$ for $T_j = 1.5T_a$. Considering the results reported for untripped jets at Mach numbers lower than or equal to 0.60 in a previous paper [11], this tone is most likely due to the fully laminar jet nozzle-exit conditions, and can be attributed to a feedback loop between the Kelvin-Helmholtz instability waves and the upstream-propagating sound waves generated by the first stage of vortex pairings in the shear layers, whose possible establishment in initially laminar free jets was proposed forty years ago by Laufer and Monkewitz [35]

and Ho and Huang [36]. Consequently, no peaks related to GJW dominate in the near-nozzle pressure spectra of the present untripped jets at $M_j = 0.60$.

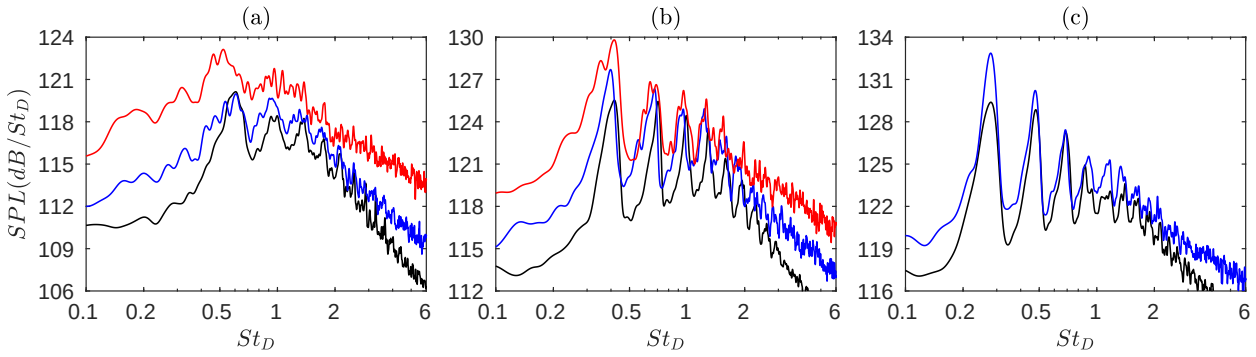

Fig. 6 Sound pressure levels at $z = 0$ and $r = 1.5r_0$ for the tripped jets at (a) $M_j \simeq 0.75$, (b) $M_j \simeq 0.90$ and (c) $M_j \simeq 1.10$ as a function of St_D: ——— $T_j = T_a$, ——— $T_j = 1.5T_a$ and ——— $T_j = 2.25T_a$.

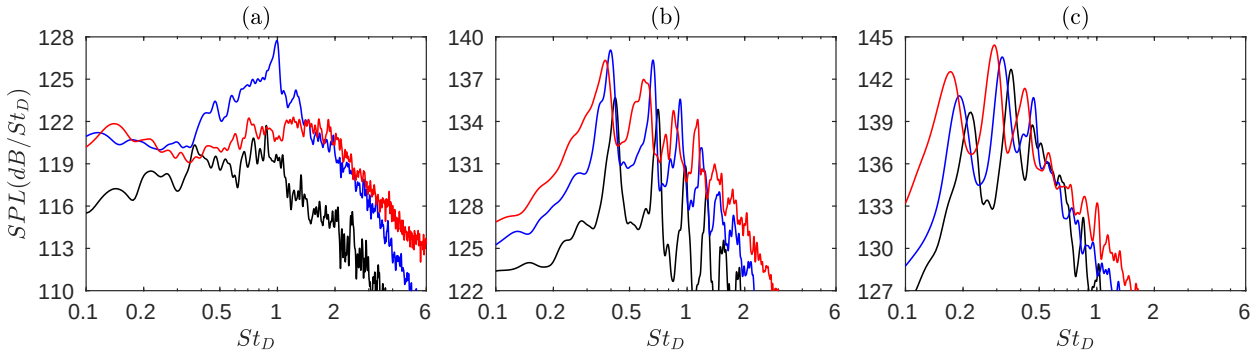

Fig. 7 Sound pressure levels at $z = 0$ and $r = 1.5r_0$ for the untripped jets at (a) $M_j = 0.60$, (b) $M_j = 0.90$ and (c) $M_j = 1.30$ as a function of St_D: ——— $T_j = T_a$, ——— $T_j = 1.5T_a$ and ——— $T_j = 2.25T_a$.

Focusing on the peak frequencies, the Strouhal numbers of the first three peaks obtained for the tripped jets at $T_j = T_a$, $T_j = 1.5T_a$ and $T_j = 2.25T_a$ for the azimuthal mode $n_\theta = 1$ are represented in figures 8(a-c) as a function of M_j between $M_j = 0.60$ and $M_j = 1.10$. As in figure 5, the allowable frequency bands of the free-stream upstream-propagating GJW and the nature of the GJW at their upper limits, predicted using a vortex-sheet model, are indicated. As noted previously, the Strouhal numbers of the peaks fall inside or near the bands, including in particular the first band for the dominant peaks. With increasing jet temperature, these bands are thicker for all Mach numbers. They also move to lower Strouhal numbers for $M_j \geq 0.90$, which is consistent with the results reported in Edgington-Mitchell and Nogueira [16] for shear layers of finite thickness. Thus, for $M_j = 1.10$ for instance, the number of bands appearing below $St_D = 2.5$ is equal to 5 in figure 8(a) for $T_j = T_a$ but to 6 in figure 8(c) for $T_j = 2.25T_a$. Regarding the changeover from a upper band limit associated with least-dispersed GJW to a limit associated with stationary GJW, it occurs at a slightly higher Mach number as the jet temperature rises. For the first radial mode, for example, it is found at $M_j = 0.80$ for $T_j = T_a$ but at $M_j = 0.87$ for $T_j = 2.25T_a$. As a result, the emergence of near-nozzle tones due to resonance between GJW in high subsonic jets is possible within narrower Mach number ranges in hot jets than in isothermal jets, in agreement with the findings in Towne et al. [1].

To better visualise the influence of the jet temperature on the peak frequencies, the peak Strouhal numbers are depicted in figures 9(a-c) for the tripped jets for the azimuthal modes $n_\theta = 0$, 1 and 2 between $M_j = 0.60$ and $M_j = 1.10$ and in figures 10(a,b) for the untripped jets for $n_\theta = 0$ and 1 between $M_j = 0.50$ and $M_j = 1.50$, along with the upper limits of the allowable frequency bands of the free-stream upstream-propagating GJW. The first three and first two peaks and GJW bands are considered for the tripped jets and for the untripped jets, respectively. For all Mach numbers, rising jet temperature appears to slightly reduce the peak Strouhal numbers, as was found in the experiments of Upadhyay & Zaman [17] for jets between $M_j = 0.90$ and $M_j = 1.20$. Above $M_j \simeq 0.80$, the decrease of the peak

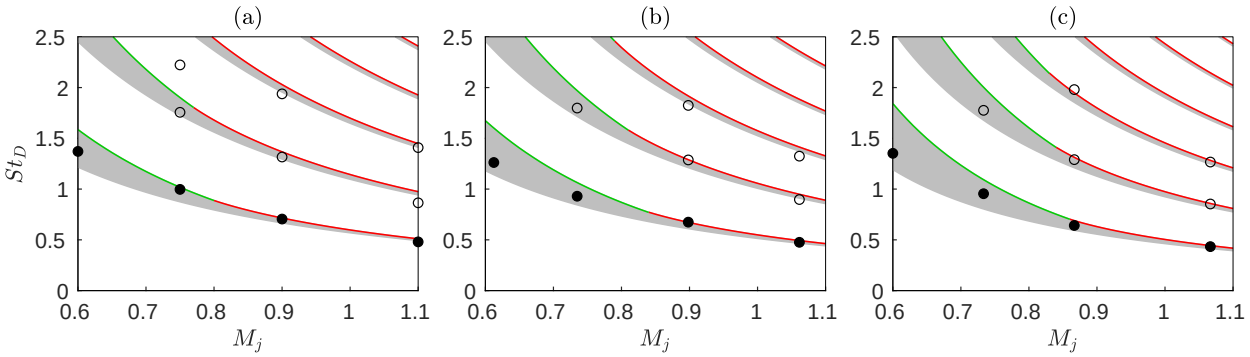

Fig. 8 Variations with M_j of the peak Strouhal numbers in the pressure spectra at $z = 0$ and $r = 1.5r_0$ for the tripped jets with (a) $T_j = T_a$, (b) $T_j = 1.5T_a$ and (c) $T_j = 2.25T_a$ for $n_\theta = 1$: • dominant and ∘ second and third strongest peaks peaks; (grey) frequency bands of the free-stream upstream-propagating GJW, upper limits of the bands corresponding to ——— stationary and ——— least-dispersed GJW.

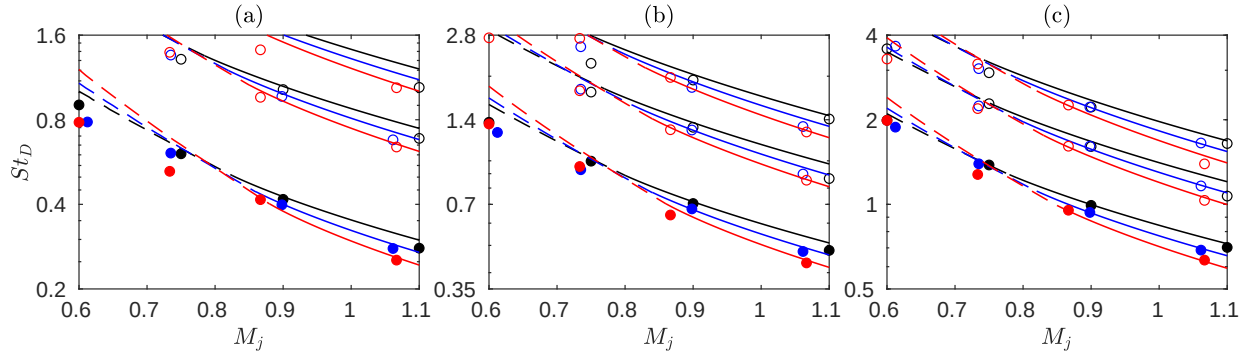

Fig. 9 Variations with M_j of the peak Strouhal numbers in the pressure spectra at $z = 0$ and $r = 1.5r_0$ for the tripped jets with (black) $T_j = T_a$, (blue) $T_j = 1.5T_a$ and (red) $T_j = 2.25T_a$ for (a) $n_\theta = 0$, (b) $n_\theta = 1$ and (c) $n_\theta = 2$: (bullets) dominant and (circles) second and third strongest peaks; upper limits of the frequency bands of the free-stream upstream-propagating GJW corresponding to (solid) stationary and (dashed) least-dispersed GJW.

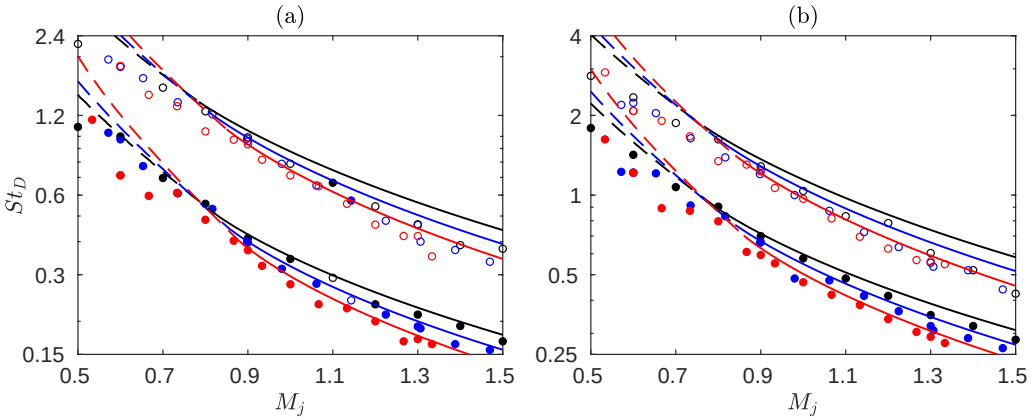

Fig. 10 Variations with M_j of the peak Strouhal numbers in the pressure spectra at $z = 0$ and $r = 1.5r_0$ for the untripped jets with (black) $T_j = T_a$, (blue) $T_j = 1.5T_a$ and (red) $T_j = 2.25T_a$ for (a) $n_\theta = 0$ and (b) $n_\theta = 1$: (bullets) dominant and (circles) second strongest GJW peaks; see caption of figure 9 for line types.

Strouhal numbers with temperature nicely follows that of the upper limits of the GJW bands, associated with stationary waves in this case. It is more pronounced at a higher Mach number. Therefore, increasing jet temperature can be expected to significantly affect the Strouhal numbers of the near-nozzle peaks and, more generally, of the resonant phenomena involving GJW, essentially at high supersonic Mach numbers. Below $M_j \simeq 0.80$, the decrease of the peak Strouhal numbers with temperature is inconsistent with the shift to higher Strouhal numbers of the band limits, associated with least-dispersed GJW in that case. This discrepancy suggests that these particular GJW do not play a key role in the generation of the near-nozzle peaks in hot jets. It could also be due to the use of a vortex-sheet model in this work, instead of a jet model with finite-thickness shear layer as was done in Tam and Ahuja [5] for a cold jet at $M_j = 0.80$ and in Edgington-Mitchell and Nogueira [16] for unheated and heated jets at $M_j \geq 0.90$, for instance.

The levels of the first two near-nozzle peaks obtained for the tripped jets for the azimuthal modes $n_\theta = 0$, 1 and 2 are represented in figures 11(a-c) as a function of M_j. Those of the dominant peaks for the untripped jets for $n_\theta = 0$ and 1 are displayed in figures 12(a,b) in the same way. In both cases, as revealed in [11] for the isothermal jets, the peak levels for the hot jets roughly grow as the eighth power of the jet velocity for $M_j \leq 1$ and as the third power for $M_j \geq 1$, in accordance with the typical scaling laws of aerodynamic noise for subsonic jets [37] and for supersonic jets [38]. This suggests that the mechanisms responsible for the peaks are of same nature regardless of the jet temperature. Moreover, the peak levels appear to be a few dB stronger for a higher temperature. In figure 11, in particular, the increases of the peak levels from $T_j = T_a$ to $T_j = 1.5T_a$ and from $T_j = 1.5T_a$ to $T_j = 2.25T_a$ are both approximately of 2 dB. These trends can be attributed to the higher velocities (and acoustic Mach numbers) of the jets when rising temperature at a fixed jet Mach number.

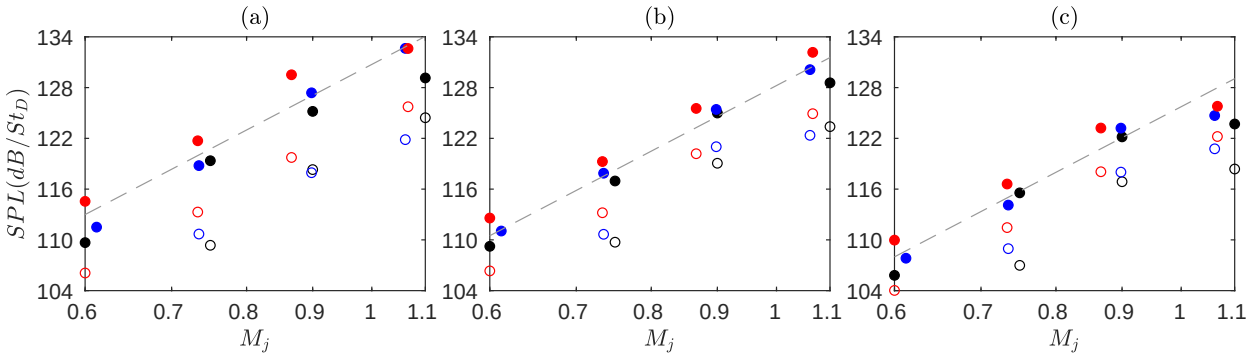

Fig. 11 Variations with M_j of the peak levels in the pressure spectra at $z = 0$ and $r = 1.5r_0$ for the tripped jets with (black) $T_j = T_a$, (blue) $T_j = 1.5T_a$ and (red) $T_j = 2.25T_a$ for (a) $n_\theta = 0$, (b) $n_\theta = 1$ and (c) $n_\theta = 2$: (bullets) dominant and (circles) second strongest peaks; – – – M_j^8.

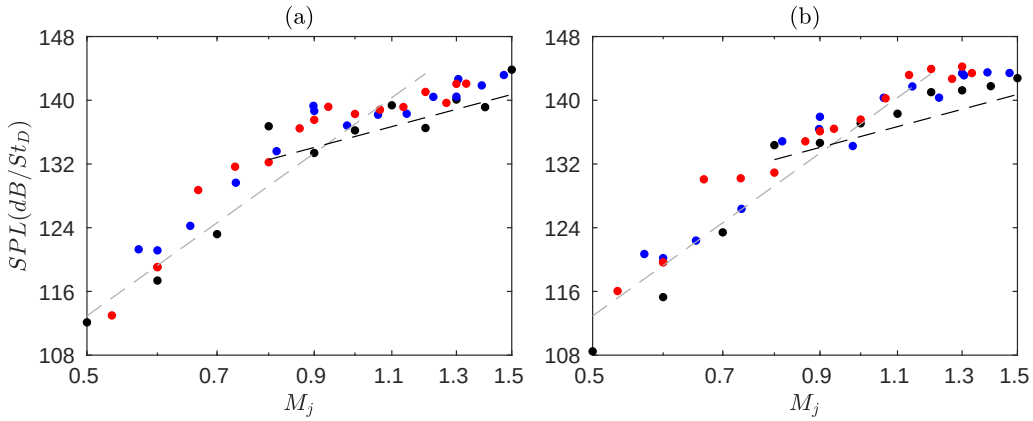

Fig. 12 Variations with M_j of the dominant GJW peak levels in the pressure spectra at $z = 0$ and $r = 1.5r_0$ for the untripped jets with (black) $T_j = T_a$, (blue) $T_j = 1.5T_a$ and (red) $T_j = 2.25T_a$ for (a) $n_\theta = 0$ and (b) $n_\theta = 1$; – – – M_j^8; – – – M_j^3.

The full widths at half maximum of the dominant near-nozzle peaks obtained for the azimuthal mode $n_\theta = 1$ are shown as a function of M_j in figure 13(a) for the tripped jets and in figure 13(b) for the untripped jets. For both nozzle-exit conditions, for $M_j < 1$, overall, the peak widths decrease with the Mach number and are larger for a higher jet temperature. These results are in good agreement with the variations of the band widths of the first radial mode of the free-stream upstream-propagating GJW for $n_\theta = 1$, also plotted given that the Strouhal numbers of the dominant near-nozzle peaks lie within the first GJW frequency band. For $M_j \geq 1$, the peak widths are small as the peaks are tonal, and they are very similar for all jet Mach numbers and temperatures.

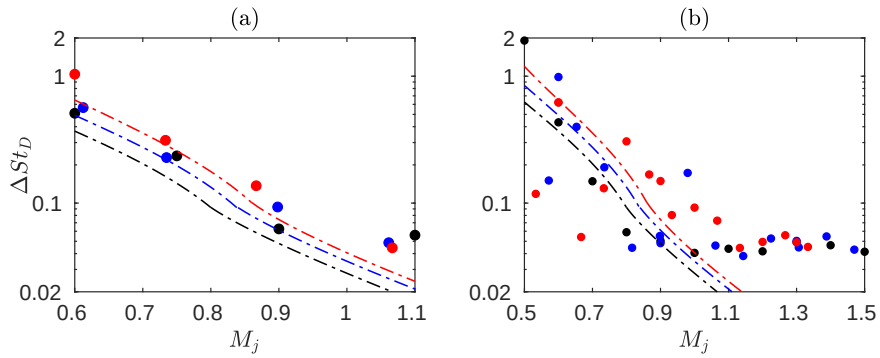

Fig. 13 Variations with M_j of the widths of the dominant GJW peaks in the pressure spectra at $z = 0$ and $r = 1.5r_0$ for $n_\theta = 1$: for the (a) tripped and (b) untripped jets for (black) $T_j = T_a$, (blue) $T_j = 1.5T_a$ and (red) $T_j = 2.25T_a$; (dashed-dotted) band width of the free-stream upstream-propagating GJW mode ($n_\theta = 1$, $n_r = 1$).

Finally, the prominences of the dominant near-nozzle peaks obtained for the untripped jets for $n_\theta = 1$ are presented in figure 13 as a function of M_j. The prominence of a peak is here defined as the difference between the peak level and the minimum level between the peak and the first next one. It is highest between $M_j \simeq 0.90$ and $M_j \simeq 1$, that is for Mach numbers for which resonant interactions can occur between upstream- and downstream-propagating GJW [1]. Both within and outside this Mach number range, the values of the peak prominence do not seem to depend on the jet temperature. This indicates that for all Mach numbers, the mechanisms generating the near-nozzle peaks have similar strengths in isothermal and hot jets.

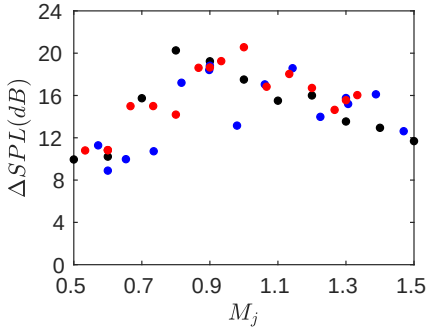

Fig. 14 Variations with M_j of the prominences of the dominant GJW peaks in the pressure spectra at $z = 0$ and $r = 1.5r_0$ for the untripped jets for (black) $T_j = T_a$, (blue) $T_j = 1.5T_a$ and (red) $T_j = 2.25T_a$.

IV. Conclusion

In this paper, the main characteristics of the acoustic peaks emerging in the near-nozzle pressure spectra of isothermal and hot jets at subsonic and supersonic Mach numbers have been investigated for a wide range of jet parameters and nozzle-exit conditions using LES. These characteristics include the peak Strouhal numbers, amplitudes, widths and prominences. Their variations with the jet velocity, Mach number and temperature have been described. For a higher jet temperature, the peak characteristics change significantly at a fixed jet velocity, but rather little at a fixed

jet Mach number. In the first case, with increasing jet temperature, the peaks are much weaker and appear at higher Strouhal numbers. In the second one, they are a few dB stronger, emerge at slightly lower Strouhal numbers and are wider for subsonic Mach numbers. Except for the decrease of the peak Strouhal numbers observed for Mach numbers lower than 0.80 at a fixed jet Mach number, these trends can be explained by the properties of the upstream-propagating free-stream GJW predicted using a vortex-sheet model. Given that, in addition, the prominence of the peaks is found not to depend on the jet temperature, the present results suggest that the mechanisms responsible for the near-nozzle acoustic peaks are of same nature and of similar strength in isothermal and hot jets. This is an important point considering that the upstream-travelling free-stream GJW producing these peaks play a key role in the feedback loops possibly establishing in free, screeching and impinging jets, and that the near-nozzle pressure peaks propagate and can be predominant in the jet acoustic far field in the upstream direction.

Acknowledgments

This work was granted access to the HPC resources of PMCS2I (Pôle de Modélisation et de Calcul en Sciences de l'Ingénieur et de l'Information) of Ecole Centrale de Lyon, and P2CHPD (Pôle de Calcul Hautes Performances Dédiés) of Université Lyon I, and to the resources of IDRIS (Institut du Développement et des Ressources en Informatique Scientifique) and TGCC (Très Grand Centre de calcul du CEA) under the allocation 2023-2a0204 made by GENCI (Grand Equipement National de Calcul Intensif). It was performed within the framework of the LABEX CeLyA (ANR-10-LABX-0060) of Université de Lyon, within the program *Investissements d'Avenir* (ANR-16-IDEX-0005) operated by the French National Research Agency (ANR).

References

[1] Towne, A., Cavalieri, A. V. G., Jordan, P., Colonius, T., Schmidt, O., Jaunet, V., and Brès, G. A., "Acoustic resonance in the potential core of subsonic jets," *J. Fluid Mech.*, Vol. 825, 2017, pp. 1113–1152. https://doi.org/10.1017/jfm.2017.346.

[2] Brès, G. A., Jordan, P., Jaunet, V., Le Rallic, M., Cavalieri, A. V. G., Towne, A., Lele, S. K., Colonius, T., and Schmidt, O. T., "Importance of the nozzle-exit boundary-layer state in subsonic turbulent jets," *J. Fluid Mech.*, Vol. 851, 2018, pp. 83–124. https://doi.org/10.1017/jfm.2018.476.

[3] Suzuki, T., and Colonius, T., "Instability waves in a subsonic round jet detected using a near-field phased microphone array," *J. Fluid Mech.*, Vol. 565, 2006, pp. 197–226. https://doi.org/10.1017/S0022112006001613.

[4] Tam, C. K. W., and Hu, F. Q., "On the three families of instability waves of high-speed jets," *J. Fluid Mech.*, Vol. 201, 1989, pp. 447–483. https://doi.org/10.1017/S002211208900100X.

[5] Tam, C. K. W., and Ahuja, K. K., "Theoretical model of discrete tone generation by impinging jets," *J. Fluid Mech.*, Vol. 214, 1990, pp. 67–87. https://doi.org/10.1017/S0022112090000052.

[6] Bogey, C., and Gojon, R., "Feedback loop and upwind-propagating waves in ideally-expanded supersonic impinging round jets," *J. Fluid Mech.*, Vol. 823, 2017, pp. 562–591. https://doi.org/10.1017/jfm.2017.334.

[7] Jordan, P., Jaunet, V., Towne, A., Cavalieri, A. V. G., Colonius, T., Schmidt, O., and Agarwal, A., "Jet–flap interaction tones," *J. Fluid Mech.*, Vol. 853, 2018, pp. 333–358. https://doi.org/10.1017/jfm.2018.566.

[8] Gojon, R., Bogey, C., and Mihaescu, M., "Oscillation modes in screeching jets," *AIAA J.*, Vol. 56, No. 7, 2018, pp. 2918–2924. https://doi.org/10.2514/1.J056936.

[9] Edgington-Mitchell, D., "Aeroacoustic resonance and self-excitation in screeching and impinging supersonic jets - A review," *Int. J. Aeroacoust.*, Vol. 18, No. 2-3, 2019, pp. 118–188. https://doi.org/10.1177/1475472X19834521.

[10] Mancinelli, M., Jaunet, V., Jordan, P., and Towne, A., "Screech-tone prediction using upstream-travelling jet modes," *Exp Fluids*, Vol. 60, No. 1, 2019, p. 22. https://doi.org/10.1007/s00348-018-2673-2.

[11] Bogey, C., "Acoustic tones in the near-nozzle region of jets: characteristics and variations between Mach numbers 0.5 and 2," *J. Fluid Mech.*, Vol. 921, 2021, p. A3. https://doi.org/10.1017/jfm.2021.426.

[12] Zaman, K. B. M. Q., Fagan, A. F., and Upadhyay, P., "Pressure fluctuations due to 'trapped waves' in the initial region of compressible jets," *J. Fluid Mech.*, Vol. 931, 2022, p. A30. https://doi.org/10.1017/jfm.2021.954.

[13] Bogey, C., "Tones in the acoustic far field of jets in the upstream direction," *AIAA J.*, Vol. 60, No. 4, 2022, pp. 2397–2406. https://doi.org/10.2514/1.J061013.

[14] Zaman, K. B. M. Q., Fagan, A. F., and Upadhyay, P., "Pressure fluctuation spectral peaks due to 'guided waves' in regions upstream of the jet exit," Tech. Rep. 2023-3649, AIAA Paper, 2023. https://doi.org/10.2514/6.2023-3649.

[15] Bogey, C., "Interactions between upstream-propagating guided jet waves and shear-layer instability waves near the nozzle of subsonic and nearly ideally expanded supersonic free jets with laminar boundary layers," *J. Fluid Mech.*, Vol. 949, 2022, p. A41. https://doi.org/10.1017/jfm.2022.776.

[16] Edgington-Mitchell, D., and Nogueira, P. A. S., "The guided-jet mode in compressible jets," Tech. Rep. 2023-3647, AIAA Paper, 2023. https://doi.org/10.2514/6.2023-3647.

[17] Upadhyay, P., and Zaman, K. B. M. Q., "Pressure fluctuations due to 'trapped waves' in heated jets," Tech. Rep. 2022-2829, AIAA Paper, 2022. https://doi.org/10.2514/6.2022-2829.

[18] Bogey, C., and Sabatini, R., "Effects of nozzle-exit boundary-layer profile on the initial shear-layer instability, flow field and noise of subsonic jets," *J. Fluid Mech.*, Vol. 876, 2019, pp. 288–325. https://doi.org/10.1017/jfm.2019.546.

[19] Bogey, C., Marsden, O., and Bailly, C., "Large-Eddy Simulation of the flow and acoustic fields of a Reynolds number 10^5 subsonic jet with tripped exit boundary layers," *Phys. Fluids*, Vol. 23, No. 3, 2011, p. 035104. https://doi.org/10.1063/1.3555634.

[20] Bogey, C., "Grid sensitivity of flow field and noise of high-Reynolds-number jets computed by large-eddy simulation," *Int. J. Aeroacoust.*, Vol. 17, No. 4-5, 2018, pp. 399–424. https://doi.org/10.1177/1475472X18778287.

[21] Mohseni, K., and Colonius, T., "Numerical treatment of polar coordinate singularities," *J. Comput. Phys.*, Vol. 157, No. 2, 2000, pp. 787–795. https://doi.org/10.1006/jcph.1999.6382.

[22] Bogey, C., de Cacqueray, N., and Bailly, C., "Finite differences for coarse azimuthal discretization and for reduction of effective resolution near origin of cylindrical flow equations," *J. Comput. Phys.*, Vol. 230, No. 4, 2011, pp. 1134–1146. https://doi.org/10.1016/j.jcp.2010.10.031.

[23] Bogey, C., and Bailly, C., "A family of low dispersive and low dissipative explicit schemes for flow and noise computations," *J. Comput. Phys.*, Vol. 194, No. 1, 2004, pp. 194–214. https://doi.org/10.1016/j.jcp.2003.09.003.

[24] Bogey, C., de Cacqueray, N., and Bailly, C., "A shock-capturing methodology based on adaptative spatial filtering for high-order non-linear computations," *J. Comput. Phys.*, Vol. 228, No. 5, 2009, pp. 1447–1465. https://doi.org/10.1016/j.jcp.2008.10.042.

[25] Berland, J., Bogey, C., Marsden, O., and Bailly, C., "High-order, low dispersive and low dissipative explicit schemes for multiple-scale and boundary problems," *J. Comput. Phys.*, Vol. 224, No. 2, 2007, pp. 637–662. https://doi.org/10.1016/j.jcp.2006.10.017.

[26] Bogey, C., and Bailly, C., "Influence of nozzle-exit boundary-layer conditions on the flow and acoustic fields of initially laminar jets," *J. Fluid Mech.*, Vol. 663, 2010, pp. 507–539. https://doi.org/10.1017/S0022112010003605.

[27] Bogey, C., and Bailly, C., "Large Eddy Simulations of transitional round jets: influence of the Reynolds number on flow development and energy dissipation," *Phys. Fluids*, Vol. 18, No. 6, 2006, p. 065101. https://doi.org/10.1063/1.2204060.

[28] Fauconnier, D., Bogey, C., and Dick, E., "On the performance of relaxation filtering for large-eddy simulation." *J. Turbulence*, Vol. 14, No. 1, 2013, pp. 22–49. https://doi.org/10.1080/14685248.2012.740567.

[29] Kremer, F., and Bogey, C., "Large-eddy simulation of turbulent channel flow using relaxation filtering: Resolution requirement and Reynolds number effects," *Comput. Fluids*, Vol. 116, 2015, pp. 17–28. https://doi.org/10.1016/j.compfluid.2015.03.026.

[30] Tam, C. K. W., and Dong, Z., "Radiation and outflow boundary conditions for direct computation of acoustic and flow disturbances in a nonuniform mean flow," *J. Comput. Acous.*, Vol. 4, No. 2, 1996, pp. 175–201. https://doi.org/10.1142/S0218396X96000040.

[31] Bogey, C., "A database of flow and near pressure field signals obtained for subsonic and nearly ideally expanded supersonic free jets using large-eddy simulations," https://hal.archives-ouvertes.fr/hal-03626787, 2022.

[32] Michalke, A., "Survey on jet instability theory," *Prog. Aerosp. Sci.*, Vol. 21, 1984, pp. 159–199. https://doi.org/10.1016/0376-0421(84)90005-8.

[33] Morris, P. J., "The instability of high speed jets," *Int. J. Aeroacoust.*, Vol. 9, No. 1-2, 2010, pp. 1–50. https://doi.org/10.1260/1475-472X.9.1-2.1.

[34] Arndt, R. E. A., Long, D. F., and Glauser, M. N., "The proper orthogonal decomposition of pressure fluctuations surrounding a turbulent jet," *J. Fluid Mech.*, Vol. 340, 1997, pp. 1–33. https://doi.org/10.1017/S0022112097005089.

[35] Laufer, J., and Monkewitz, P., "On turbulent jet flows: a new perspective," Tech. Rep. 80-0962, AIAA Paper, 1980. https://doi.org/10.2514/6.1980-962.

[36] Ho, C.-M., and Huang, L.-S., "Subharmonics and vortex merging in mixing layers," *J. Fluid Mech.*, Vol. 119, 1982, pp. 443–473. https://doi.org/10.1017/S0022112082001438.

[37] Lighthill, M. J., "On sound generated aerodynamically I. General theory," *Proc. Roy. Soc. A*, Vol. 211, No. 1107, 1952, pp. 564–587. https://doi.org/10.1098/rspa.1952.0060.

[38] Ffowcs Williams, J. E., "The noise from turbulence convected at high speed," *Phil. Trans. R. Soc. Lond. A*, Vol. 255, No. 1061, 1963, pp. 469–503. https://doi.org/10.1098/rsta.1963.0010.